

The roles of external forcing and natural variability in global warming hiatuses

Lei Zhang¹ 

Received: 23 August 2015 / Accepted: 2 February 2016 / Published online: 8 February 2016
© Springer-Verlag Berlin Heidelberg 2016

Abstract Global mean surface temperature (GMST) rising has slowed down since late 1990s, which is referred to as the global warming hiatus. There was another global warming hiatus event during 1940s–1960s. The roles of the external forcing and the natural variability in both global warming hiatuses are explored, using EOF analysis. The first two leading EOF modes of the 5-year running mean global sea surface temperature (SST) reflect the global warming scenario (EOF1) and the interdecadal Pacific oscillation (IPO)-like natural variability (EOF2), respectively. In observation, PC2 was in its positive phase (eastern Pacific cooling) during 1940s–1960s, which contributed to the previous warming hiatus. In addition, GMST trends are found to be negative during late 1950s and 1960s in most of the CMIP5 historical runs, which implies that the external forcing also contributed to the pause in the GMST rising. It is further demonstrated that it is the natural radiative forcing (volcanic forcing) that caused the drop-down of GMST in 1960s. The current global warming hiatus has been attributed to the eastern Pacific cooling/enhanced Pacific trade winds. It is shown that the PC2 switched to its positive phase in late 1990s, and hence the IPO-like natural variability made a contribution to the slowdown of GMST rising in the past decade. It is also found that the EOF1 mode (global warming mode) of the observed SST features a smaller warming

in tropical Pacific compared to the Indian Ocean and the tropical Atlantic. Such inter-basin warming contrast, which is attributed to the “ocean thermostat” mechanism, has been suggested to contribute to the intensification of Pacific trade winds since late 1990s as well. Global warming hiatuses are also found in the future projections from CMIP5 models, and the spatial pattern of the SST trends during the warming-hiatus periods exhibits an IPO-like pattern, which resembles the observed SST trends since late 1990s.

Keywords Global warming hiatus · EOF analysis of global SST · External forcing and natural variability

1 Introduction

Global mean surface temperature (GMST) has been rising steadily at a rate of 0.1–0.15 K decade⁻¹ during the recent decades (IPCC 2007), owing to the effects of greenhouse gases (GHG) associated with the anthropogenic activities. The GHG effect-induced changes of the climate system have been widely studied (e.g. Meehl et al. 2005; Vecchi et al. 2006; Knutson et al. 2010). It is also found that the surface warming trend has slowed down since late 1990s such that the linear GMST trend during the past 15 years is nearly zero (e.g. Kosaka and Xie 2013; Trenberth and Fasullo 2013). Concerns about whether this phenomenon indicates that the global warming is no longer happening have been raised by the public ever since, but many studies have suggested that the slowdown of GMST rising is only temporary and so it is now often referred to as “the global warming hiatus” (e.g. Easterling and Wehner 2009; Meehl et al. 2011; Kosaka and Xie 2013; Trenberth and Fasullo 2013; Trenberth et al. 2014).

Electronic supplementary material The online version of this article (doi:[10.1007/s00382-016-3018-6](https://doi.org/10.1007/s00382-016-3018-6)) contains supplementary material, which is available to authorized users.

✉ Lei Zhang
lezh8230@colorado.edu

¹ Cooperative Institute for Research in Environmental Sciences, University of Colorado, Boulder, CO, USA

An important question is what causes the global warming hiatus. Previous studies have attributed this phenomenon to the decreases in stratospheric water vapor (Solomon et al. 2010) and solar radiation (Kaufmann et al. 2011), and increases in stratospheric aerosols (Solomon et al. 2011). However, the radiative forcing (RF) at the top of atmosphere remained positive (around 0.5–1 W/m²) in the past decade (Trenberth and Fasullo 2013). Furthermore, it is found that on top of an evident warming trend, global warming hiatuses show up in climate models forced by increasing GHGs (e.g. Easterling and Wehner 2009; Meehl et al. 2011; Watanabe et al. 2014), and some studies have shown that the natural variability plays an important role in the current global warming hiatus (e.g. England et al. 2014; Trenberth et al. 2014). Li et al. (2013) found that the North Atlantic Oscillation (NAO) leads the variability of northern-hemisphere mean surface temperature by 15–20 years through delayed impact on the Atlantic Multidecadal Oscillation (AMO), and this process contributed to the slowing down of northern hemisphere warming trend since 2000. The delayed effect of the NAO on the AMO is further confirmed in Sun et al. (2015a, b). Many studies have also demonstrated that the current warming hiatus seems related to the eastern pacific (EP) cooling anomaly/enhanced Pacific trade winds. Kosaka and Xie (2013) showed that by forcing their model with observed tropical EP sea surface temperatures (SST), the trends of which exhibited a La-Nina like pattern since the year 2000, the temporal evolution of the GMST since 1970s was very well simulated, including the current global warming hiatus. Merrifield (2011) found that the Walker circulation has been strengthening over the past decade, and England et al. (2014) showed that the slowdown of surface warming trend since late 1990s was reproduced in their numerical simulations when the Pacific trade winds were prescribed as the observed patterns.

What caused the EP SST cooling/enhanced Pacific trade winds in the past decade? Natural variability in tropical Pacific may probably play an important role (e.g. Trenberth et al. 2014). In addition, McGregor et al. (2014) concluded that the anomalous SST warming in the tropical Atlantic may lead to enhanced trade winds over the equatorial Pacific. Luo et al. (2012) pointed out that the relatively faster warming rate in the Indian Ocean (IO) compared to the tropical Pacific over the past few decades might contribute to the intensification of the Pacific trade winds as well. What caused the inter-basin warming contrast, however, remains unclear.

In addition to the current warming hiatus, it is also noted that the GMST warming trend was nearly zero or even negative during 1940s–1960s (Figs. 1, 2, 3). Analysis of this previous warming hiatus may help improve our

understanding of the observed climate changes. It has been argued in previous literatures that the slowdown of GMST rising in the middle of twentieth century might be attributed to the external forcing (e.g. Clement and Dinezio 2014). However, as shown below, the natural variability might play a role in the previous global warming hiatus as well.

The causes of the previous and the current global warming hiatuses are explored in this study by analyzing both the observational datasets and the coupled model inter-comparison project phase 5 (CMIP5) historical runs (Sect. 4). Prediction of the future climate is of vital importance, and therefore the future projections from CMIP5 models under the representative concentration pathway 4.5 (RCP4.5) scenario are analyzed to evaluate the ability of the coupled climate models to simulate the global warming hiatus (Sect. 5). In RCP4.5, the radiative forcing reaches 4.5 W m⁻² (equivalent to 650 ppm CO₂ concentration) in 2100 and stabilizes after that.

2 Data and method

The reconstructions of SST datasets for the period of 1900–2013 from Hadley center (HadISST, Rayner et al. 2003), extended range SST from NOAA (ERSST, Smith et al. 2008) and Kaplan et al. (1998) were employed in this study. Because of different instrumental measurements (e.g. using water from buckets or ship engine room; whether satellite retrievals are used or not), the three SST datasets exhibit some different characteristics, which are discussed in the following sections. In addition to the observed SST datasets, the CMIP5 model simulations are analyzed as well. 125 historical simulations for the period of 1900–2005 from 34 CMIP5 models are used (Table 1). To evaluate the ability of the climate models to simulate the warming hiatuses, future projections from 31 CMIP5 climate models under RCP4.5 scenario (2006–2100) are analyzed. To reveal the role of the external forcing in the previous warming hiatus, RF of both the anthropogenic forcing (AF) and the natural forcing are analyzed.

To identify the leading modes of global SST variability, empirical orthogonal function (EOF) analysis was performed, which has been used in numerous previous studies to extract the dominant modes of SST variability (e.g. Folland et al. 1999; Parker et al. 2007; Zhang et al. 2010; Hartmann 2015). Prior to the EOF analysis, a 5-year running mean filter was applied to the annual mean SST field to remove the evident interannual variabilities such as El Nino-Southern Oscillation (ENSO). To reveal the main features of the GMST evolution, 10-year running trends of GMST were calculated for both the observations and the CMIP5 models, and a 5-year running mean filter was also applied to GMST prior to the calculation.

3 EOF modes of global SST

Figures 1, 2 and 3 show the first two leading EOF modes of the annual mean global SST for different datasets, and the spatial patterns between 60°N and 60°S are shown. The interannual variabilities were effectively removed by applying a 5-year running mean filter prior to the EOF analysis. The EOF1 (EOF2) mode accounts for more than 50 % (10 %) of the variance (Table 2). EOF3 mode explains 7–8 % of the variance, but there are substantial discrepancies among the EOF3 modes for the three SST datasets (Fig. S1), and the correlation coefficients between PC3s are not as significant as PC2s (Table S1). Therefore, only the first two EOF modes are analyzed here.

3.1 EOF1 mode: global warming mode

EOF1 modes for the three SST datasets are similar, which show nearly ubiquitous SST warming globally (Figs. 1a, 2a, 3a). PC corresponding to the EOF1 mode mainly exhibits a rising trend since 1900 (Figs. 1d, 2d, 3d), which matches the global mean SST evolution very well (Figs. 1c, 2c, 3c). PC1s for different SST datasets are highly correlated (~0.98, Table 3). Thus, the EOF1 mode of the smoothed global SST primarily reflects the global warming scenario. Note that the rising trend in PC1 stagnated during 1940s–1960s (Figs. 1d, 2d, 3d), corresponding to a global warming hiatus that can be found in the evolution of global mean SST as well (Figs. 1c, 2c, 3c).

Fig. 1 Spatial patterns of **a** EOF1 mode and **b** EOF2 mode of the smoothed global SST for HadISST (unit: K). **c** Domain averaged annual mean SST anomaly (unit: K). *Black* for area weighted global mean SST anomalies, *blue* for eastern Pacific region (180° – 80° W, 20° S– 20° N), *red* for tropical Atlantic (60° W– 0° , 20° S– 20° N) and *green* for the Indian Ocean (40° E– 120° E, 20° S– 20° N). **d** PCs corresponding to the EOF1 (solid) and EOF2 (dashed) mode

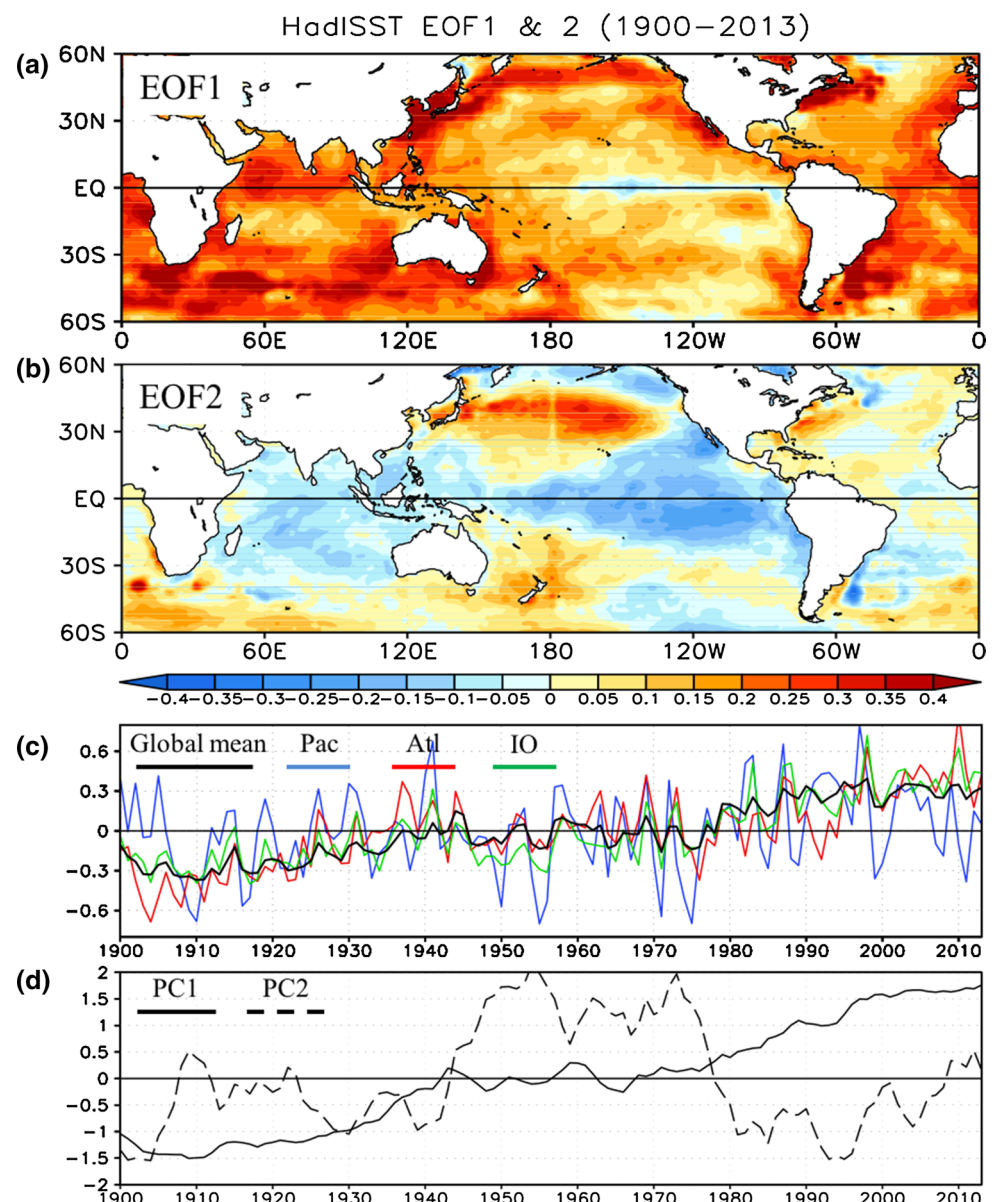
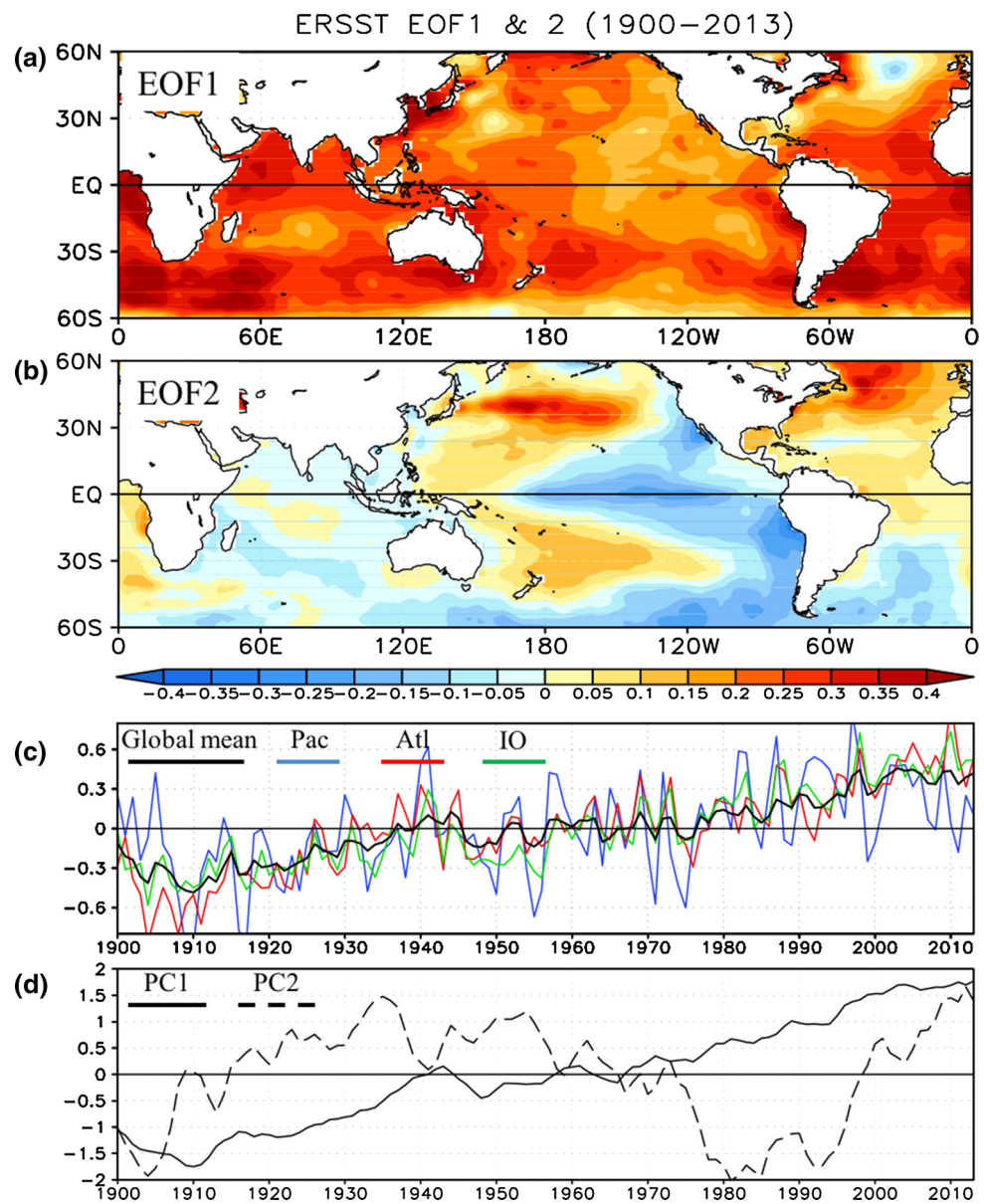


Fig. 2 Same as Fig. 1, but for ERSST



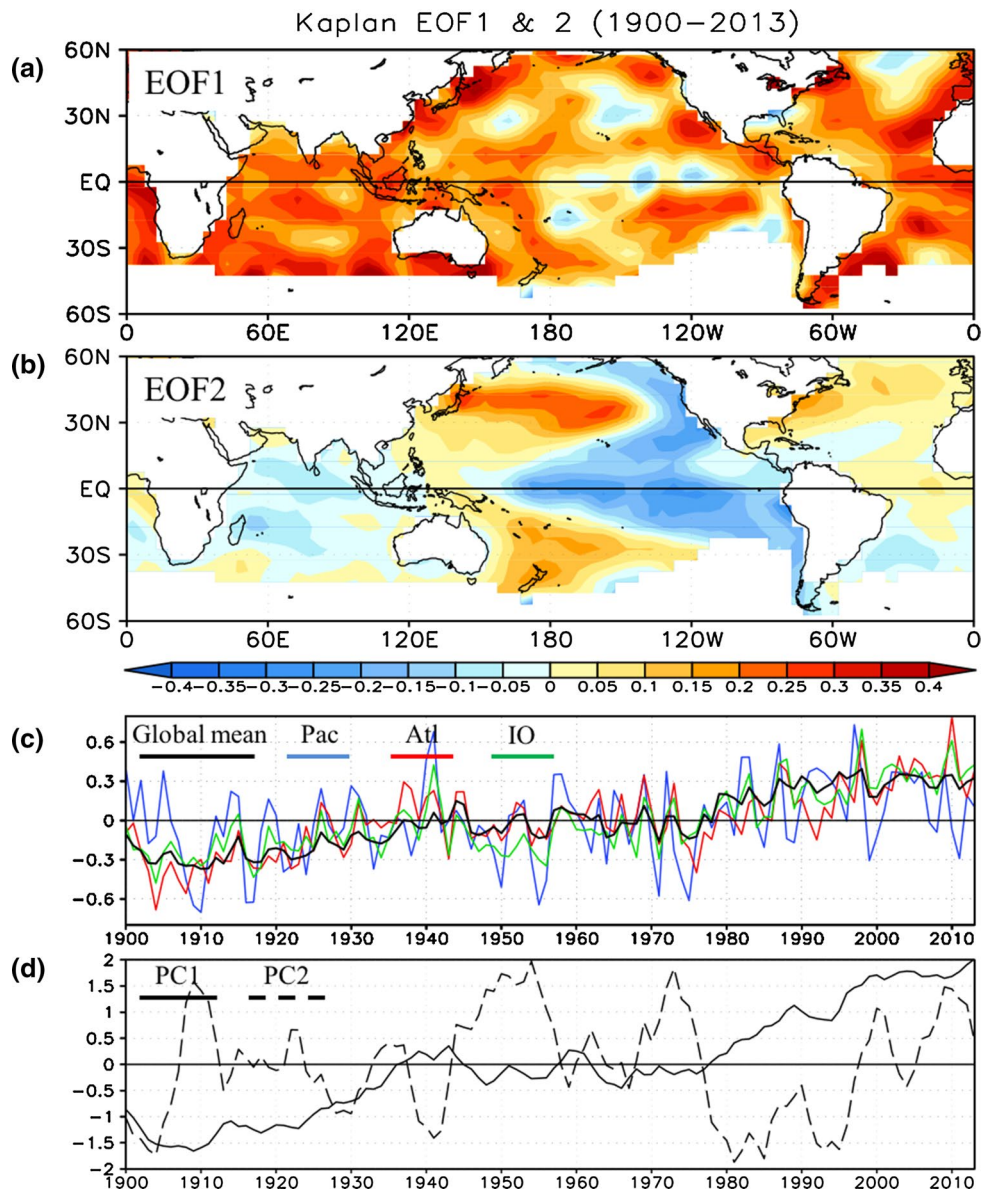
It is interesting to note that the EOF1 mode shows greater SST warming in the IO and the tropical Atlantic compared to the Pacific region. The time series of the domain-averaged SST anomalies also show that the warming rate in Pacific fell behind that in the other two basins since late 1990s (Figs. 1c, 2c, 3c). As suggested in previous studies, these inter-basin warming contrasts contributed to the enhanced Pacific trade winds in the past decade. The physical mechanism for the less Pacific SST warming is discussed in Sect. 4. It is also noted that the EOF1 mode exhibits increased east–west SST gradient in the equatorial Pacific (Figs. 1a, 2a, 3a). This is in contrast to the previous finding that the CMIP5 models predominantly simulate an El Niño like SST warming in response to the GHG-effect (e.g. Xie et al. 2010). Nevertheless, the

consistency among the EOF1 modes for different SST datasets is clear.

3.2 EOF2 mode: IPO-like mode

Figures 1b, 2b and 3b show the second leading EOF mode of the smoothed global SST. The most remarkable features of the EOF2 mode are the pronounced negative SST anomalies in tropical EP and the positive SST anomalies in mid-latitude Pacific in both hemispheres. Sun et al. (2013) performed EOF analysis on zonal mean global SST and found a symmetric mode that is pronounced in the Pacific, which is similar to the EOF2 mode found here. The spatial pattern of the EOF2 mode resembles the interdecadal Pacific oscillation (IPO) identified in previous literatures (e.g. Zhang

Fig. 3 Same as Fig. 1, but for Kaplan SST dataset



et al. 1997; Power et al. 1999), which is similar to ENSO but with a broader latitudinal extent. PC corresponding to the EOF2 mode indeed exhibits strong variabilities on an inter-decadal time scale (Figs. 1d, 2d, 3d), with a positive phase during 1940s–1970s and a negative phase from late 1970s to late 1990s. The PC2s for the three SST datasets are also well correlated (Table 3). However, there are some discrepancies in PC2s for the three SST datasets. For instance, PC2 stayed in its positive phase till 1970s in Fig. 1d, whereas the PC2 for ERSST transited to its negative phase in mid 1960s (Fig. 2d). There are strong fluctuations in PC2 during the previous warming hiatus in Fig. 3d. The discrepancies in PC2s were more evident before 1950s, which might be due to the sparse observations in that time period (Deser et al. 2010). It is also interesting to see that there is large Atlantic

loading in the EOF2 mode for ERSST, but such feature cannot be found in the other two SST datasets.

Different from the EOF1 mode, the EOF2 mode shows much less pronounced SST anomalies in the IO and the tropical Atlantic: SST anomalies in IO are nearly zero in Fig. 2b, whereas Figs. 1b and 3b show relatively evident IO cooling; anomalous tropical Atlantic warming shows up in the EOF2 modes for ERSST and Kaplan SST (Figs. 2b, 3b), but SST anomalies in tropical Atlantic are insignificant in Fig. 1b.

3.3 CMIP5 historical runs

EOF analysis was also performed on the SST field between 60°N and 60°S from the CMIP5 historical runs

Table 1 34 CMIP5 climate models used in this study for analysis (125 ensemble members)

Model	Modeling center (Group)	AGCM resolution	Ensemble No.
ACCESS1-0	The Centre for Australian Weather and Climate Research	$1.875^\circ \times 1.25^\circ$	1
ACCESS1-3		$1.875^\circ \times 1.25^\circ$	1
BCC-CSM1-1	Beijing Climate Center, China Meteorological Administration	$2.8125^\circ \times 2.8125^\circ$	3
BCC-CSM1-1-M	Beijing Climate Center, China Meteorological Administration	$1.125^\circ \times 1.125^\circ$	1
BNU-ESM	College of Global Change and Earth System Science, Beijing Normal University	$2.8125^\circ \times 2.8125^\circ$	1
CMCC-CESM	Centro Euro-Mediterraneo per I Cambiamenti Climatici	$3.75^\circ \times 3.75^\circ$	1
CMCC-CMS		$1.875^\circ \times 1.875^\circ$	1
CNRM-CM5	Centre National de Recherches Meteorologiques/ Centre Europeen de Recherche et Formation Avancees en Calcul Scientifique	$1.40625^\circ \times 1.40625^\circ$	10
CNRM-CM5-2			1
CSIRO-Mk3-6-0	Commonwealth Scientific and Industrial Research Organization in collaboration with Queensland Climate Change Centre of Excellence	$1.875^\circ \times 1.875^\circ$	1
CSIRO-Mk3L-1-2		$5.625^\circ \times 3.214^\circ$	3
CanESM2	Canadian Centre for Climate Modelling and Analysis	$2.8125^\circ \times 2.8125^\circ$	5
FGOALS-g2	LASG, Institute of Atmospheric Physics, Chinese Academy of Sciences	$2.8125^\circ \times 3^\circ$	1
GFDL-CM2p1	NOAA Geophysical Fluid Dynamics Laboratory	$2.5^\circ \times 2^\circ$	10
GFDL-CM3			5
GFDL-ESM2 M			1
GISS-E2-H	NASA Goddard Institute for Space Studies	$2.5^\circ \times 2^\circ$	18
GISS-E2-H-CC			1
GISS-E2-R			24
GISS-E2-R-CC			1
HadGEM2-CC	Met Office Hadley Centre	$1.875^\circ \times 1.24^\circ$	1
HadGEM2-ES			2
INMCM4	Institute for Numerical Mathematics	$2^\circ \times 1.5^\circ$	1
IPSL-CM5A-LR	Institut Pierre-Simon Laplace	$3.75^\circ \times 1.875^\circ$	6
IPSL-CM5A-MR		$2.5^\circ \times 1.258^\circ$	3
IPSL-CM5B-LR		$3.75^\circ \times 1.875^\circ$	1
MIROC-ESM-CHEM	Japan Agency for Marine-Earth Science and Technology, Atmosphere and Ocean Research Institute (The University of Tokyo), and National Institute for Environmental Studies	$2.8125^\circ \times 2.8125^\circ$	1
MIROC-ESM			3
MIROC5	Atmosphere and Ocean Research Institute (The University of Tokyo), National Institute for Environmental Studies, and Japan Agency for Marine-Earth Science and Technology	$1.40625^\circ \times 1.40625^\circ$	5
MPI-ESM-LR	Max Planck Institute for Meteorology	$1.875^\circ \times 1.875^\circ$	3
MPI-ESM-MR			3
MPI-ESM-P			2
NorESM1-M	Norwegian Climate Centre	$2.5^\circ \times 1.875^\circ$	3
NorESM1-ME			1

Monthly SST data are analyzed

Table 2 Percentage of the variance explained by the first two leading EOF modes of the SST field from observational datasets and CMIP5 historical runs

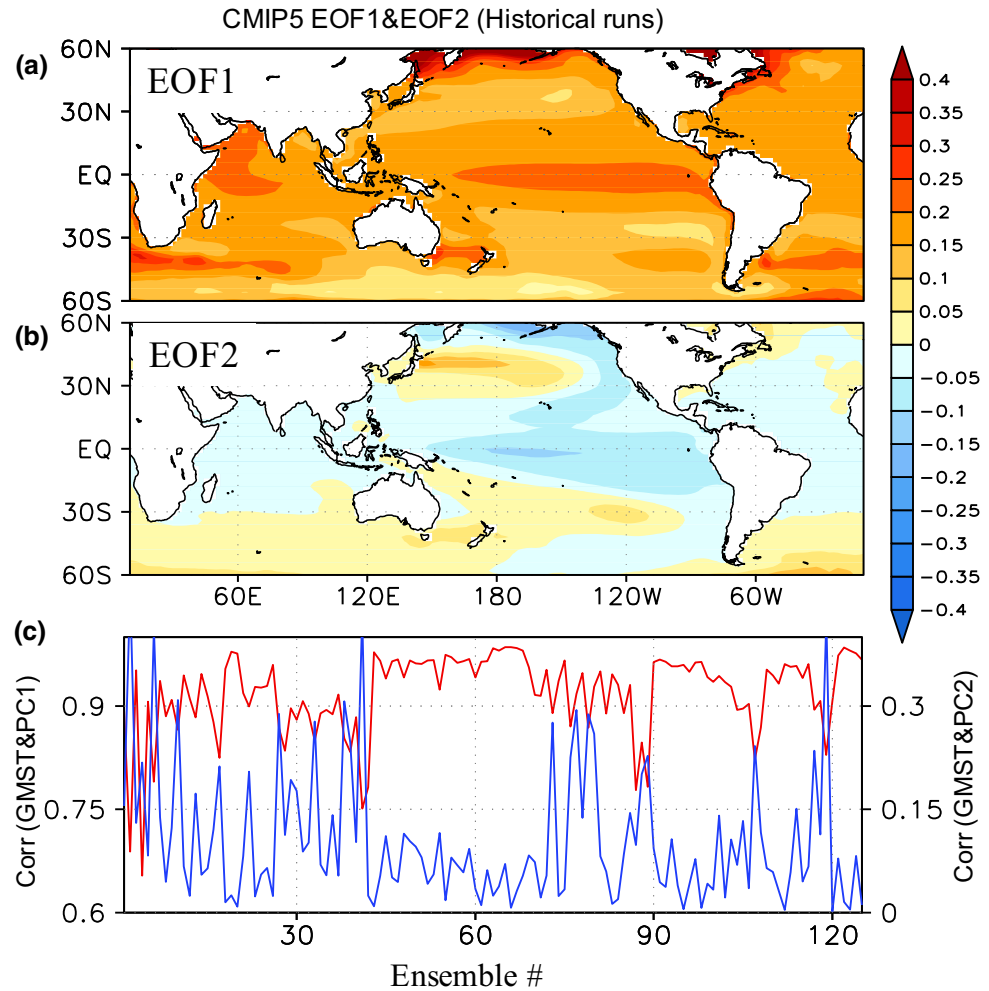
	ERSST (%)	HADISST (%)	Kaplan (%)	CMIP5 (%)
EOF1	56.7	54.9	52.9	45.5
EOF2	10.6	10.6	11.2	11.8

(Fig. 4). EOF1 (EOF2) mode explains around 45 % (11 %) of the variance on average (Table 2). To be consistent, the EOF1 mode is defined as the global mean SST anomalies being positive, and the EOF2 mode is defined as SST anomalies in tropical EP region being negative. PCs corresponding to these two modes are adjusted accordingly.

Table 3 PC correlation coefficients between the three observational SST datasets analyzed in this study

	PC1			PC2		
	Hadley	ERSST	Kaplan	Hadley	ERSST	Kaplan
Hadley	1.00	0.99	0.98	1.00	0.48	0.80
ERSST		1.00	0.98		1.00	0.72
Kaplan			1.00			1.00

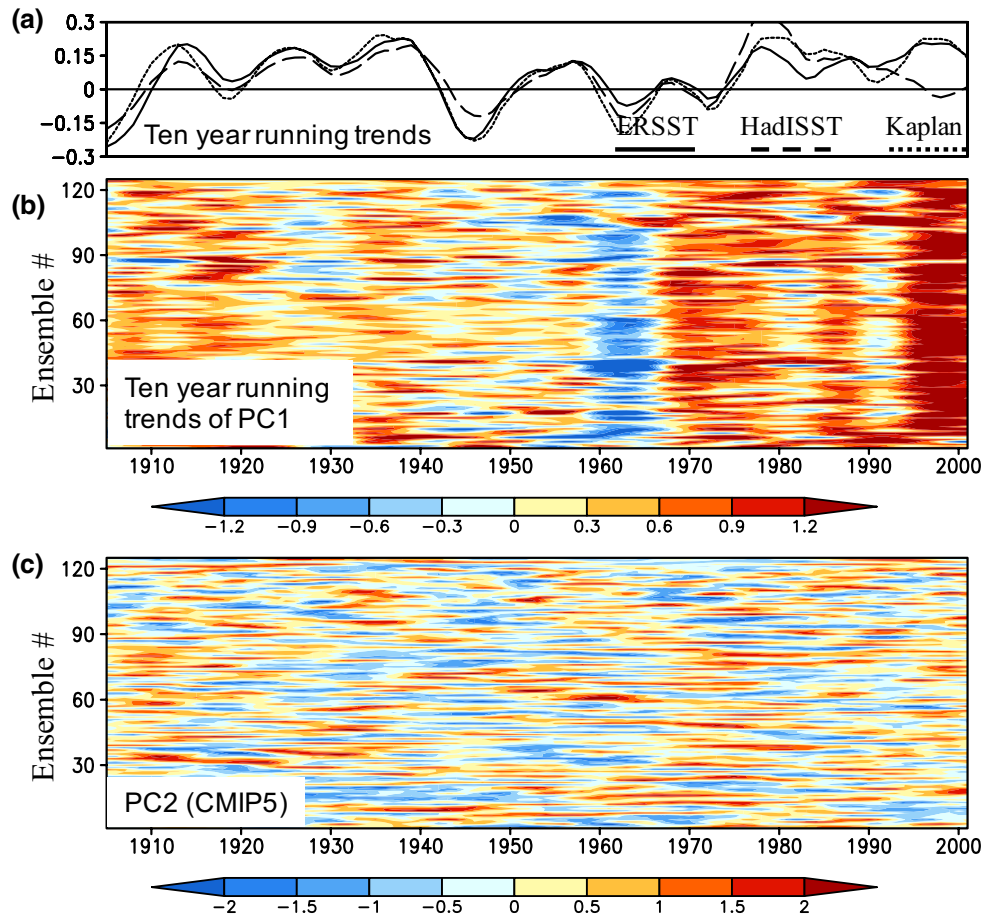
Fig. 4 Spatial patterns of the ensemble mean **a** EOF1 mode and **b** EOF2 mode of the smoothed SST between 60°N and 60°S from CMIP5 historical runs (unit: K). **c** The correlation coefficients between GMST and PC1 (red curve, left axis) and the absolute value of correlation coefficients between GMST and PC2 (blue curve, right axis) for the ensemble members



EOF1 mode still presents as ubiquitous SST warming (Fig. 4a), and the correlation coefficient between GMST and PC1 reaches around 0.9 in most of the ensemble members (Fig. 4c). Ensemble mean EOF2 mode exhibits an IPO-like pattern (Fig. 4b), which resembles the EOF2 mode of the observed SST (Figs. 1b, 2b, 3b), and the correlation coefficient between GMST and PC2 is insignificant (Fig. 4c). The spectral analysis reveals that the significant period of the PC2 is beyond 10 years (figure not shown). Thus, same as the observational datasets, the first two leading EOF modes of SST from CMIP5 historical runs primarily describe the global warming scenario (EOF1) and the IPO-like natural variability on an interdecadal time scale (EOF2), respectively.

In contrast to the similarities between the EOF2 modes for observations and CMIP5 historical runs, the spatial pattern of the EOF1 mode in Fig. 4a is distinctly different from those in Figs. 1a, 2a and 3a. For CMIP5 historical runs, EOF1 mode exhibits greater SST warming in Pacific than either IO or tropical Atlantic and an El Niño-like SST warming in equatorial Pacific (Fig. 4a). In contrast, Pacific SST warming is clearly smaller than the other two basins and the east–west SST gradient in tropical Pacific increases in Figs. 1a, 2a and 3a. The main features of the EOF1 mode (global warming mode) shown in Fig. 4a are consistent with the previous studies that found an enhanced equatorial warming and an El Niño-like warming in tropical Pacific

Fig. 5 **a** Ten year running trends of 5-year running mean global mean SST for ERSST (solid), HadISST (dashed) and Kaplan SST (dotted) (units: K decade $^{-1}$). **b** Ten-year running trends of PC1s for the ensemble members from CMIP5 historical runs, unit decade $^{-1}$ (y-axis represents ensemble member). **c** PC2s for the same ensemble as in **b**



in the projections from CMIP5 climate models (e.g. Vecchi et al. 2008; Xie et al. 2010; Zhang and Li 2014). It is important and interesting to explore the reasons for such prominent discrepancies between the models and the observations, but it is beyond the scope of this study.

It is noted that the EOF2 and EOF1 modes in Fig. 4 are similar to Fig. 3c, d in Watanabe et al. (2014), respectively. In their study, the natural variability and the GHG-forced signals were obtained from the control run and the sensitivity experiment forced by increasing GHGs, respectively.

4 Global warming hiatuses

In this section, the roles of the external forcing and the natural variability in the slowdown of global warming during both the previous and the current warming hiatus periods are explored by analyzing the observational SST datasets and CMIP5 historical runs.

4.1 Previous warming hiatus

It is illustrated in Sect. 3 that there was a previous global warming hiatus during 1940s–1960s (Figs. 1c, 2c, 3c). The

10-year running trends of global mean SST are shown in Fig. 5a, which indeed shows negative trends in 1940s and 1960s. It is noted that the PC2 was in its positive phase (EP cooling) during the previous warming hiatus period (Figs. 1d, 2d, 3d), albeit the discrepancies in the PC2s for different datasets. As pointed out by Kosaka and Xie (2013), the evident EP cooling anomaly may lead to the slowdown of GMST rising. Hence, the IPO-like natural variability associated with the EOF2 mode indeed contributed to the previous warming hiatus during 1940s–1960s. After late 1970s, PC2 transited into its negative phase (Figs. 1d, 2d, 3d), contributing to the pronounced rising trend in GMST that primarily caused by the increases in GHGs.

In addition to the natural variability, the role of the external forcing in the previous warming hiatus is also explored here by analyzing the 10-year running trends of GMST in a large ensemble of CMIP5 historical runs. Since the initial condition varies across the ensemble members of the CMIP5 models, the phases of the natural variabilities are expected to be different among the ensemble members. Indeed, Fig. 5c, which shows the PC corresponding to the EOF2 mode, is characterized by pronounced discrepancies among different ensemble members. This suggests that one

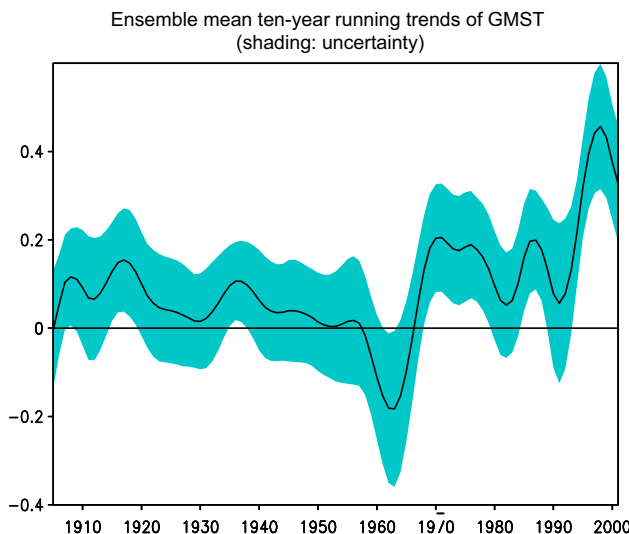


Fig. 6 Ensemble mean 10-year running trends of 5-year running mean GMST in CMIP5 historical runs (units: K decade⁻¹). Shading represents the uncertainty, which is defined as one standard deviation across the ensemble members

may find coherent GMST trends across most of the ensemble members only when the external forcing plays a dominant role. As shown in Figs. 5b and 6, there were negative trends in both PC1s and GMSTs in most of the CMIP5 historical runs over the period of late 1950s and 1960s, during which there was an observed warming hiatus (Fig. 5a). The running trends then became positive since 1970s, which is consistent with the observed rapid rise in GMST during the recent decades due to the GHG effect. This result suggests that both the previous warming hiatus during late 1950s and 1960s and the accelerated warming between late 1970s and late 1990s were largely contributed by the external forcing. It is also noted that there were evident negative trends in the observed GMST in 1940s (Fig. 5a), yet the trends in GMST are inconsistent among the ensemble members of CMIP5 historical runs in that time period (Fig. 5b). Thus, the natural variability might play an important role in the early period of the previous warming hiatus. Indeed, as discussed above, PC2 was in its positive phase in 1940s (EP cooling, Figs. 1, 2, 3), which contributed to the negative GMST trend.

To reveal the cause of the negative external forcing in 1960s, Fig. 7 shows the time evolution of the RF of both anthropogenic forcing and natural forcing. It is found that the AF increased steadily during the previous warming hiatus due to the GHG effect, despite decreases in the RF of aerosols (Fig. 7a). In contrast, total RF dropped sharply and became negative in 1960s due to the inclusion of the natural forcing. Moreover, in CMIP5 simulations that are forced only by the natural forcing, one can find negative GMST trends over the period of late 1950s and 1960s in

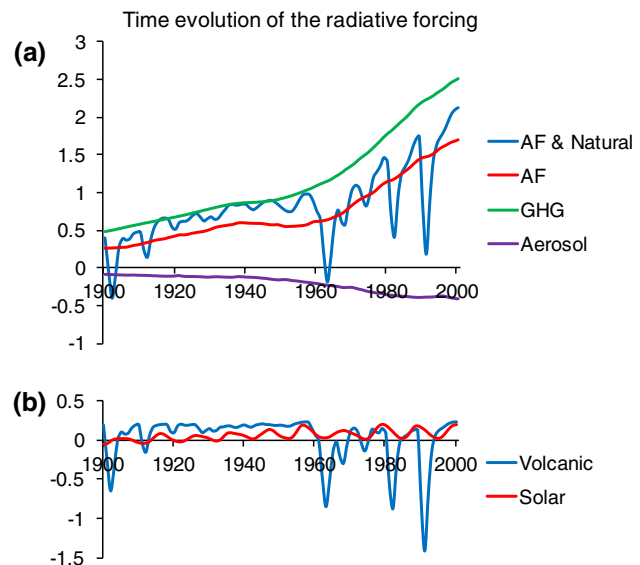


Fig. 7 **a** Time evolution of the annual averaged, global mean radiative forcing of anthropogenic forcing plus natural forcing (blue), anthropogenic forcing only (red), greenhouse gas forcing (green) and the direct forcing of aerosols (purple) (units: W m⁻²). **b** Same as **a** but for volcanic forcing (blue) and solar irradiance (red)

most of the ensemble members (figure not shown). Hence it is the natural forcing that contributed to the downward trend in both the external forcing and the GMST during late 1950s and 1960s. Figure 7b further shows the volcanic forcing and the solar irradiance, the two important components of the natural forcing, and it is found that the variability of the natural forcing is predominantly controlled by the volcanic forcing, whereas the solar irradiance only shows a regular 11-year cycle. Note that the low values in the volcanic forcing in 1960s, 1980s and early 1990s are all consistent with those in the total RF (Fig. 7a). There were two major volcanic eruptions during late 1950s and 1960s, i.e., the eruptions of volcano Bezymianny and volcano Mount Agung, the volcanic explosivity index of which were both five, which might contribute to the evident negative trends in the volcanic forcing during late 1950s and 1960s.

Figures 8a–f shows the spatial patterns of SST trends over the periods of 1940–1950 and 1958–1968, during which there were evident negative GMST trends in observations (Fig. 5a). Pronounced tropical EP cooling trends showed up during 1940–1950 (Figs. 8a–c), which is similar to the EOF2 mode identified in the previous sections (Figs. 1b, 2b, 3b). This confirms that the IPO-like natural variability contributed to the warming hiatus in 1940s. In contrast, the spatial pattern of SST trends during 1958–1968 manifested itself quite differently, i.e., the SST cooling was more uniformly distributed and no IPO-like pattern could be found (Figs. 8d–f). The discrepancies between the SST trends during the two periods confirm that the negative

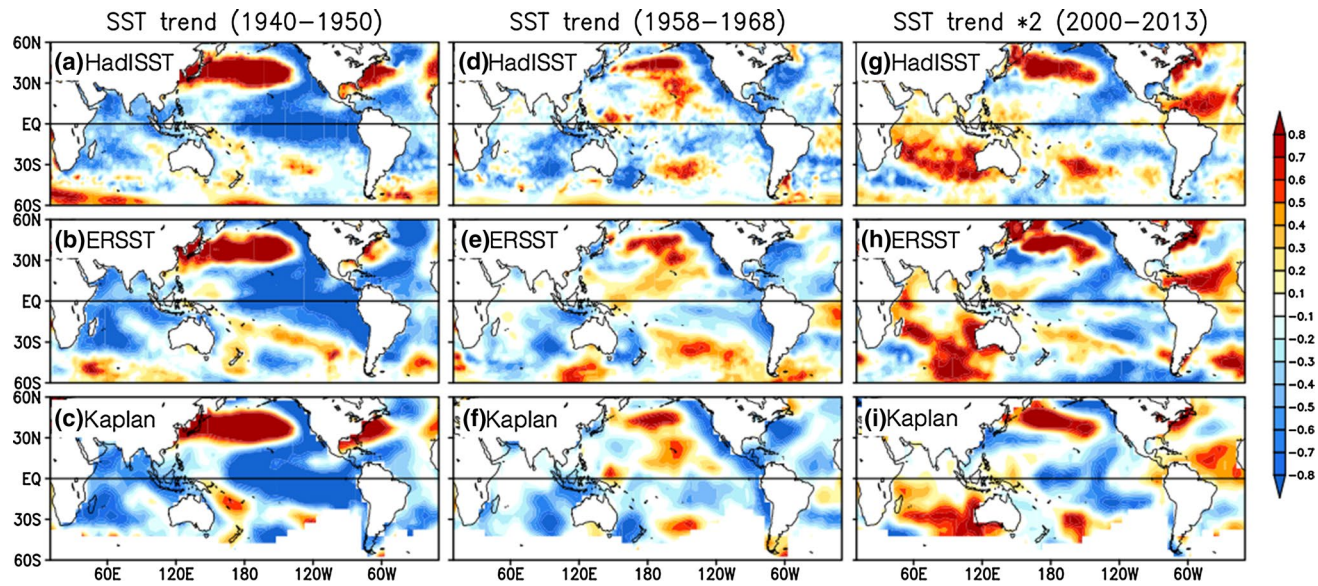


Fig. 8 Spatial patterns of SST trends over the period of **a–c** 1940–1950, **d–f** 1958–1968 and **g–i** 2000–2013. Units are K decade^{-1} for 1940–1950 and 1958–1968, and $0.5 \text{ K decade}^{-1}$ for 2000–2013. Results for the three observational SST datasets analyzed in this study are shown

trends in GMST during 1940s and 1960s are attributed to different processes. SST trends during 1958–1968 in CMIP5 historical runs are also examined, the pattern of which exhibits nearly ubiquitous SST cooling throughout the global ocean surface (Figure S2). This is profoundly different from the SST trends during the warming hiatuses in the models, which show an IPO-like pattern with evident EP cooling (Fig. 9). These results suggest that the externally forced warming hiatus manifests itself differently from the warming hiatus associated with the IPO-like natural variability.

4.2 Current warming hiatus

It is pointed out that the GMST rising has slowed down since 2000, which is further linked to the EP cooling/enhanced Pacific trade winds. The spatial pattern of the observed SST trends during 2000–2013 exhibits an IPO-like pattern (Figs. 8g–i), i.e., substantial EP cooling trend and positive SST trends in mid-latitude Pacific. Consistently, PC2s for ERSST and Kaplan SST transited into their positive phases in late 1990s (Figs. 2d, 3d), although the phase transition of PC2 occurs later in Fig. 1d. Therefore, the recent EP cooling trend seems related to the IPO-like EOF2 mode, which is consistent with the previous finding (e.g. England et al. 2014; Trenberth et al. 2014).

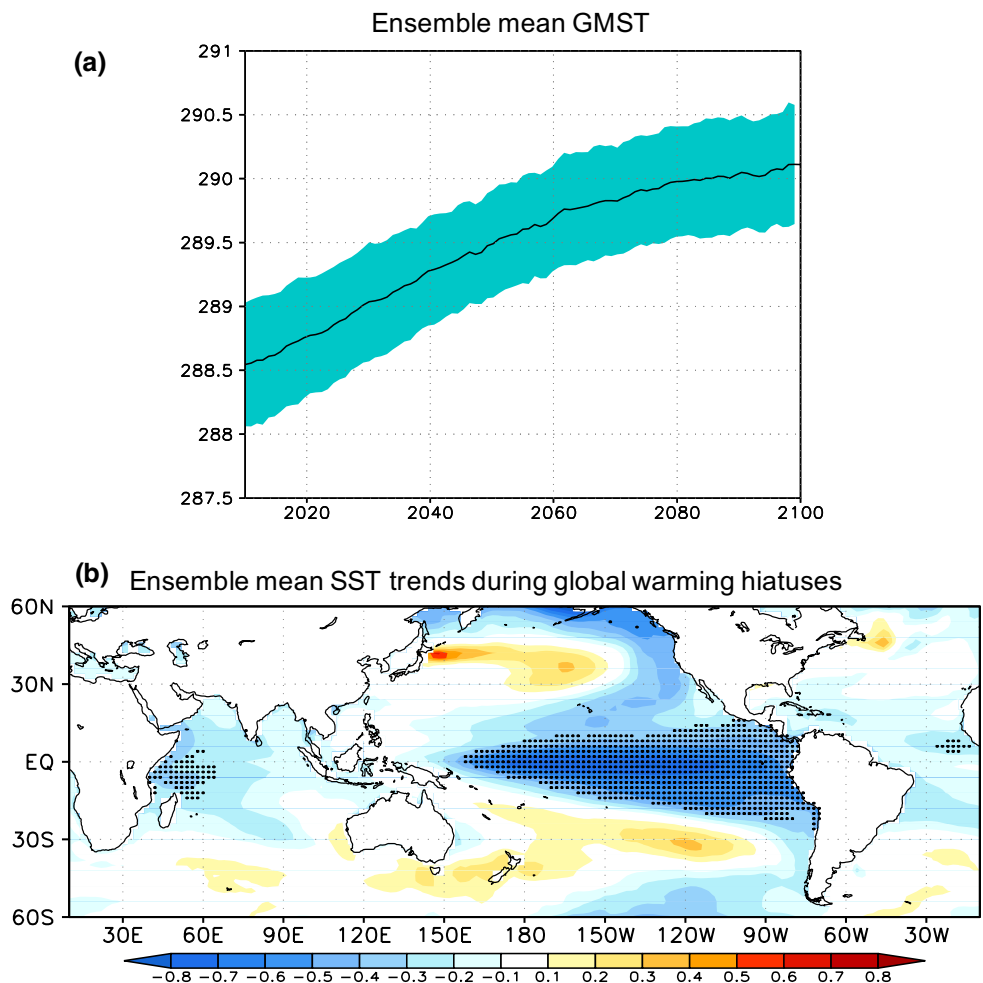
In addition to the role of the IPO-like natural variability in the current warming hiatus, previous studies have also demonstrated that the inter-basin warming contrasts, i.e., greater SST warming in the IO and the tropical Atlantic than the tropical Pacific, contributed to the intensification of Pacific trade

winds in the past decade as well (Luo et al. 2012; McGregor et al. 2014). As illustrated in Sect. 3, the EOF1 mode of the observed SST indeed shows less Pacific warming compared to the other two ocean basins (Figs. 1a, 2a, 3a). Since the EOF1 mode essentially depicts the global warming scenario, it is important to understand what physical mechanism gives rise to the observed inter-basin warming contrasts under global warming. Clement et al. (1996) proposed the “ocean thermostat” mechanism, based on which a La Niña-like SST warming in response to the GHG effect was predicted. They argued that under global warming, the strong oceanic upwelling in tropical EP brings up the cold water underneath and cools the surface. This oceanic upwelling damping weakens the EP SST warming and leads to a stronger east–west SST gradient in the equatorial Pacific, which further strengthens the low-level trade winds. The air-sea interaction subsequently amplifies the EP cooling/enhanced Pacific trade winds. Such ocean dynamic constraint limits the Pacific SST warming in a warmer climate and hence contributed to the inter-basin warming contrasts in the past decade. The “ocean thermostat” mechanism may also help explain the increased east–west SST gradient in the EOF1 mode of the observed SST (Figs. 1a, 2a, 3a). Zhang et al. (2010) found a SST cooling mode associated with pronounced EP cooling, which they also attributed to the GHG effect and the ocean dynamical damping.

5 Future projections

The future projections from CMIP5 RCP4.5 experiments are analyzed to evaluate the ability of the climate models to

Fig. 9 **a** Evolution of the ensemble mean GMST (unit: K) in CMIP5 RCP4.5 experiments, shading represents one standard deviation across the ensemble members (unit: K). **b** Ensemble mean SST trends during the warming hiatus periods in CMIP5 RCP4.5 experiments (units: K decade $^{-1}$). Stippled area are the regions where SST trends during at least 178 events (80 % of total 222 events) agree with the sign of the ensemble mean SST trends



simulate the global warming hiatuses. Figure 9 shows the ensemble mean results from 63 ensemble members. GMST increases at a rate of 0.16 ± 0.05 K decade $^{-1}$ in response to the increasing GHGs (Fig. 9a). By calculating the 10-year running trends of GMST, it is found that near zero or even negative trends indeed show up in the 95-year simulation from the CMIP5 models. To obtain the robust signals during the warming hiatus events, the periods during which the GMST trend is smaller than -0.1 K decade $^{-1}$ were picked out, and 48 out of 63 ensemble members capture such events. This criterion is the same as that used in Meehl et al. (2011). 4–5 warming hiatus events are captured in each ensemble member on average. The ability of the models to simulate the warming hiatus does not seem model-dependent. For instance, some of the ensemble members of GISS-E2-R capture the warming hiatuses, while others do not. It seems that the initial condition may be an important factor, which is consistent with the finding in Meehl and Teng (2014).

Figure 9b shows the ensemble mean SST trends during 222 warming hiatus events, in which the stippled areas are the regions where the SST trends during at least 178 events

(80 % of the total 222 events) agree with the sign of the ensemble mean SST trends. The most remarkable feature of the SST trends during these hiatus events is the evident cooling trends in the EP region, which is consistent with the observed SST trends during the current global warming hiatus (Fig. 8g–i) and the EOF2 modes of both the observed (Figs. 1b, 2b, 3b) and model SST (Fig. 4b). This result suggests that the warming hiatuses that are linked to the IPO-like natural variability can be captured by the climate models. Previous studies also suggested that the general circulation models could simulate the current warming hiatus reasonably well, given proper initialization and bias adjustment (e.g. Meehl and Teng 2014).

6 Conclusions

We explored the roles of the external forcing and the natural variability in the slowdown of the GMST rising by performing the EOF analysis on the smoothed global SST field. It is found that for both observations and CMIP5 models, the EOF1 mode presents as nearly ubiquitous SST

warming, and PC1 is highly correlated with the time evolution of GMST. Thus, the first leading mode essentially describes the global warming scenario. The second EOF mode mainly reflects the IPO-like natural variability on an interdecadal time scale.

It is shown that the PC2 was in its positive phase (EP cooling) during 1940s–1960s, and therefore, the IPO-like EOF2 mode contributed to the drop-down of GMST during the previous global warming hiatus period. In addition, GMST trends are found to be negative over the period of late 1950s and 1960s in most of the ensemble members of the CMIP5 historical runs, which implies that the external forcing made a contribution to the previous warming hiatus as well. It is further demonstrated that the negative trend in radiative forcing during late 1950s and 1960s was primarily attributed to the volcanic forcing. Between late 1970s and late 1990s, PC2 was in its negative phase, which contributed to the accelerated warming that primarily caused by the GHG effect.

PC2 transited into its positive phase in late 1990s, and hence the IPO-like EOF2 mode contributed to the current warming hiatus. It is also found that the EOF1 mode (global warming mode) of the observed SST exhibits less Pacific warming than the IO and the tropical Atlantic. As suggested in previous studies, such inter-basin warming contrasts also contributed to the enhanced Pacific trade winds and the warming hiatus in the past decade. The less Pacific warming is attributed to the oceanic upwelling damping mechanism (Clement et al. 1996).

Analysis of the future projections from CMIP5 models reveals that the coupled climate models are capable of simulating the warming hiatuses, during which the spatial pattern of SST trends is characterized by pronounced EP cooling, similar to the observed SST trends over the past decade and the EOF2 modes of both observed and model SST.

It is noted that the EOF1 modes of the observed and model SST manifest themselves profoundly differently, i.e., Pacific warming is smaller (greater) compared to the tropical Atlantic and the IO, and the zonal SST gradient in the equatorial Pacific is enhanced (weakened) in the EOF1 mode in observations (CMIP5 historical runs). Given the substantial impact of the tropical Pacific on the global climate system, the cause of the prominent discrepancies between the observations and the climate model simulations is worth examined in a future study. In addition, since it has been shown that both the inter-basin warming contrasts and the IPO-like natural variability made contributions to the enhanced Pacific trade winds during the current warming hiatus, it would be interesting to explore the relative importance of these two mechanisms in the intensification of Pacific trade winds over the past decade as well.

Acknowledgments I am grateful to the anonymous reviewers for their constructive comments on the original manuscript. I acknowledge the World Climate Research Program's Working Group on Coupled Modeling, which is responsible for CMIP, and I thank the climate modeling groups for producing and making available their model outputs.

References

- Clement A, DiNezio P (2014) The Tropical Pacific Ocean—back in the driver's seat? *Science* 343:976–978
- Clement AC, Seager R, Cane MA, Zebiak SE (1996) An ocean dynamical thermostat. *J Clim* 9:2190–2196
- Deser C, Phillips AS, Alexander MA (2010) Twentieth century tropical sea surface temperature trends revisited. *Geophys Res Lett.* doi:[10.1029/2010GL043321](https://doi.org/10.1029/2010GL043321)
- Easterling DR, Wehner MF (2009) Is the climate warming or cooling? *Geophys Res Lett.* doi:[10.1029/2009GL037810](https://doi.org/10.1029/2009GL037810)
- England MH, McGregor S, Spence P et al (2014) Recent intensification of wind-driven circulation in the Pacific and the ongoing warming hiatus. *Nat Clim Change* 4:222–227
- Folland CK, Parker DE, Colman AW, Washington R (1999) Large scale modes of ocean surface temperature since the late nineteenth century. Springer, Berlin Heidelberg, pp 73–102
- Hartmann DL (2015) Pacific sea surface temperature and the winter of 2014. *Geophys Res Lett* 42:1894–1902
- IPCC Climate Change (2007) The physical science basis. Contribution of Working Group I to the Fourth Assessment Report of the Intergovernmental Panel on Climate Change. Edited by Solomon S et al. Cambridge University Press, Cambridge, United Kingdom and New York, NY, USA.
- Kaplan A, Cane M, Kushnir Y, Clement A, Blumenthal M, Rajagopalan B (1998) Analyses of global sea surface temperature 1856–1991. *J Geophys Res* 103:567–589
- Kaufmann RK, Kauppi H, Mann ML et al (2011) Reconciling anthropogenic climate change with observed temperature 1998–2008. *Proc Natl Acad Sci* 108:11790–11793
- Knutson TR, McBride JL, Chan J, Emanuel K, Holland G, Landsea C, Held IM, Kossin JP, Srivastava AK, Sugi M (2010) Tropical cyclones and climate change. *Nat Geosci* 3:157–163
- Kosaka Y, Xie SP (2013) Recent global-warming hiatus tied to equatorial Pacific surface cooling. *Nature* 501:403–407
- Li JP, Sun C, Jin F-F (2013) NAO implicated as a predictor of Northern Hemisphere mean temperature multidecadal variability. *Geophys Res Lett* 40:5497–5502
- Luo JJ, Sasaki W, Masumoto Y (2012) Indian Ocean warming modulates Pacific climate change. *Proc Natl Acad Sci* 109:18701–18706
- McGregor S, Timmermann A, Stuecker MF et al (2014) Recent Walker circulation strengthening and Pacific cooling amplified by Atlantic warming. *Nat Clim Change* 4:888–892
- Meehl GA, Teng H (2014) CMIP5 multi-model hindcasts for the mid-1970s shift and early 2000s hiatus and predictions for 2016–2035. *Geophys Res Lett* 41:17111716. doi:[10.1002/2014GL059256](https://doi.org/10.1002/2014GL059256)
- Meehl GA et al (2005) How much more global warming and sea level rise? *Science* 307:1769–1772
- Meehl GA, Arblaster JM, Fasullo JT et al (2011) Model-based evidence of deep-ocean heat uptake during surface-temperature hiatus periods. *Nat Clim Change* 1:360–364
- Merrifield MA (2011) A shift in western tropical Pacific sea level trends during the 1990s. *J Clim* 24:4125–4138
- Parker D, Folland C, Scaife A, Knight J, Colman A, Baines P, Dong B (2007) Decadal to multidecadal variability and the climate

- change background. *J Geophys Res Atmos* 1984–2012:112. doi:10.1029/2007JD008411
- Power S, Casey T, Folland C, Colman A, Mehta V (1999) Inter-decadal modulation of the impact of ENSO on Australia. *Clim Dyn* 15:319–324
- Rayner NA, Parker DE, Horton EB, Folland CK, Alexander LV, Rowell DP, Kent EC, Kaplan A (2003) Global analyses of sea surface temperature, sea ice, and night marine air temperature since the late nineteenth century. *J Geophys Res.* doi:10.1029/2002JD002670
- Smith TM, Reynolds RW, Peterson TC, Lawrimore J (2008) Improvements to NOAA's historical merged land-ocean surface temperature analysis (1880–2006). *J Clim* 21:2283–2296
- Solomon S, Rosenlof KH, Portmann RW et al (2010) Contributions of stratospheric water vapor to decadal changes in the rate of global warming. *Science* 327:1219–1223
- Solomon S, Daniel JS, Neely RR et al (2011) The persistently variable “background” stratospheric aerosol layer and global climate change. *Science* 333:866–870
- Sun C, Li JP, Jin F-F, Ding QR (2013) Sea surface temperature inter-hemispheric dipole and its relation to tropical precipitation. *Environ Res Lett.* doi:10.1088/1748-9326/8/4/044006
- Sun C, Li JP, Jin F-F (2015a) A delayed oscillator model for the quasi-periodic multidecadal variability of the NAO. *Clim Dyn.* doi:10.1007/s00382-014-2459-z
- Sun C, Li JP, Feng J, Xie F (2015b) A decadal-scale teleconnection between the north atlantic oscillation and subtropical eastern Australian rainfall. *J Clim* 28:1074–1092
- Trenberth KE, Fasullo JT (2013) An apparent hiatus in global warming? *Earth's Future* 1:19–32
- Trenberth KE, Fasullo JT, Branstator G, Phillips AS (2014) Seasonal aspects of the recent pause in surface warming. *Nat Clim Change.* doi:10.1038/NCLIMATE2341
- Vecchi GA, Soden BJ, Wittenberg AT, Held IM, Leetmaa A, Harrison MJ (2006) Weakening of tropical Pacific atmospheric circulation due to anthropogenic forcing. *Nature* 441:73–76
- Vecchi GA, Clement A, Soden BJ (2008) Examining the tropical Pacific's response to global warming. *Eos* 89:81–83
- Watanabe M, Shiogama H, Tatebe H et al (2014) Contribution of natural decadal variability to global warming acceleration and hiatus. *Nat Clim Change* 4:893–897
- Xie SP, Deser C, Vecchi GA, Ma J, Teng H, Wittenberg AT (2010) Global warming pattern formation: sea surface temperature and rainfall. *J Clim* 23:966–986
- Zhang L, Li T (2014) A simple analytical model for understanding the formation of sea surface temperature patterns under global warming. *J Clim* 27:8413–8421
- Zhang Y, Wallace JM, Battisti DS (1997) ENSO-like interdecadal variability: 1900–93. *J Clim* 10:1004–1020
- Zhang W, Li J, Zhao X (2010) Sea surface temperature cooling mode in the Pacific cold tongue. *J Geophys Res* 115:C12042. doi:10.1029/2010JC006501